Percolation and nanosecond fluctuators in V_2O_3 films within the metal–insulator transition

Cite as: APL Mater. 8, 101103 (2020); doi: 10.1063/5.0023475
Submitted: 29 July 2020 • Accepted: 9 September 2020 •
Published Online: 1 October 2020

Liyang Chen,[1] Panpan Zhou,[2] Yoav Kalcheim,[3] Ivan K. Schuller,[3] and Douglas Natelson[1,2,4,5,a)]

AFFILIATIONS

[1]Applied Physics Graduate Program, Rice University, Houston, Texas 77005, USA
[2]Department of Physics and Astronomy, Rice University, Houston, Texas 77005, USA
[3]Faculty of Materials Science and Engineering Technion, Israel Institute of Technology, Haifa 32000, Israel
[4]Department of Electrical and Computer Engineering, Rice University, Houston, Texas 77005, USA
[5]Department of Materials Science and NanoEngineering, Rice University, Houston, Texas 77005, USA

[a)]**Author to whom correspondence should be addressed:** natelson@rice.edu

ABSTRACT

Vanadium sesquioxide (V_2O_3) exhibits a metal–insulator transition (MIT) at 160 K between a low temperature, monoclinic, antiferromagnetic Mott insulator and a high temperature, rhombohedral, paramagnetic, metallic phase. In thin films, a percolative transition takes place over a finite temperature range of phase coexistence. We study the fluctuating dynamics of this percolative MIT by measuring voltage noise spectra at both low frequencies (up to 100 kHz) and radio frequencies (between 10 MHz and 1 GHz). Noise intensity quadratic in bias is observed in the MIT region, as expected for resistive fluctuations probed nonperturbatively by the current. The low frequency noise resembles flicker-type $1/f^{\beta}$ noise, often taking on the form of Lorentzian noise dominated by a small number of fluctuators as the volume fraction of the insulating phase dominates. Radio frequency noise intensity also quadratic in the bias current allows the identification of resistance fluctuations with lifetimes below 1 ns, approaching timescales seen in non-equilibrium pump–probe studies of the transition. We find quantitative consistency with a model for fluctuations in the percolative fraction. The thermodynamics of the MIT suggests that dominant fluctuations are ones that alter small volumes affecting the connectivity of domain boundaries. This noise serves as a sensitive and nonperturbative probe for the dynamics of switching phenomena in this system.

I. INTRODUCTION

The study of phase transitions remains at the core of physics. Vanadium sesquioxide (V_2O_3), as an archetypal material with strong electronic correlations, undergoes a rhombohedral paramagnetic metal to monoclinic antiferromagnetic insulator transition when cooled below 160 K, with films showing a temperature range of phase coexistence of ~30 K.[1] The resistance increases by several orders of magnitude with cooling as antiferromagnetic insulating domains grow at the expense of paramagnetic metallic domains. The metal–insulator transition (MIT) may be triggered by several stimuli, such as temperature,[2] light,[3,4] strain,[5] pressure,[6] and electric field.[7] Ultrafast optical pump–probe methods have shown that the non-equilibrium photo-induced phase transition can happen within 100 ps, while some experiments show that non-equilibrium phase precursors appear during a photo-excited insulator-to-metal transition within 2.5 ps.[9] The thermally driven dynamics in the equilibrium phase and the mixed phase regime remain comparatively unstudied. Increased interest in such metal–insulator materials for neuromorphic computing applications[10] has emphasized the importance of understanding fluctuations in the transition, both in and out of equilibrium.

In inhomogeneous material systems with networks of conducting and insulating regions, resistance fluctuations have proven to be a powerful tool for examining the transition between bulk metallicity and insulating response in the context of percolation.[11–17] Resistive noise can also give insights into localization in nominally homogeneous materials close to the Anderson transition.[18,19]

Low-frequency resistive noise measurements have been performed in correlated materials with metal–insulator transitions, such as $La_{5/8-x}Pr_xCa_{3/8}MnO_3$,[20] $La_{2/3}Ca_{1/3}MnO_3$,[21] and vanadium dioxide.[22] Studies in the correlated materials have largely focused on the percolative nature of the mixed-phase regime, with some insights into how the frequency dependence of the resistive noise can arise from correlations.[23]

The "flicker" voltage noise spectrum from resistance fluctuations typically has a spectral density (mean square voltage fluctuations per unit bandwidth) $S(f) \sim 1/f^{\beta}$, where f is the frequency and β is close to 1. For an ohmic device with resistance R, one can convert interchangeably between voltage noise $S_V(f)$ (V^2/Hz) and current noise $S_I(f) = S_V(f)/R^2$ (A^2/Hz). This is the well-known $1/f$ noise that has been found in almost all devices and materials.[24–26] One reason for the seeming ubiquity of the $1/f$ functional form for the spectral density is that it can result from the added contributions of individual fluctuators. An individual resistive fluctuator with a characteristic lifetime $1/f_c$ contributes[25] a component to the noise with a Lorentzian frequency dependence $S(f) \propto f_c/(f_c^2 + f^2)$. A linear combination of several fluctuators of comparable amplitudes with broadly distributed lifetimes results in a total $S(f) \sim 1/f$ over the relevant frequency range. Lorentzian deviations from $S(f) \sim 1/f^{\beta}$ are observed when the noise response is dominated by one or more particular fluctuators.[27] The intensity of $1/f$ noise can be characterized[26] for comparison between different material systems via the normalized voltage noise, $(S_V/(IR)^2)v_s f = \alpha/n$, where v_s is the volume of the sample, I is the bias current, R is the average sample resistance, α is Hooge's parameter,[28] and n is a density of fluctuators, usually assumed to be the carrier density.

Here, we report measurements of the intrinsic, thermally driven resistance fluctuations in the mixed phase regime of the V_2O_3 metal–insulator transition via noise spectra measured under sufficiently small, non-perturbative bias currents. We extend the frequency range of noise measurements up to 1 GHz and find resistive fluctuations (noise intensity quadratic in measurement current) up to several hundred megahertz. This implies the existence of nanosecond fluctuators, a timescale comparable to those found in experiments probing the nonequilibrium metal–insulator transition.[8] Lorentzian-like roll-offs are seen at the upper limit of our frequency range, and particularly toward the insulating regime, indicating that noise can be dominated by a small number of fluctuators. The noise magnitude as a function of device resistance is consistent with a 2D percolation model based on fluctuations in the percolating fraction. However, the data imply that it is unlikely that fluctuation-driven transitions of entire domains between metallic and insulating states are at work. In devices with the largest current density, the dependence of the noise intensity with bias current becomes superquadratic, implying that sufficiently large currents can perturb the dynamics of the fluctuators.

II. EXPERIMENT

A. Device fabrication

V_2O_3 thin films 100 nm-thick were grown epitaxially on r-cut sapphire substrates by RF magnetron sputtering deposition. Structural characterization of such films has been described extensively elsewhere.[29,30] For transport measurements, 70 nm thick Au electrodes (6 nm V adhesion layer) were patterned by electron beam lithography, electron beam evaporation, and liftoff. After lithography and development, the exposed surface was cleaned by Ar plasma (9 W) for 1 min before electrode deposition. The ratio of width to height of each electrode gap is fixed to 1:4 for all device sizes, with an example shown in Fig. 1(a). The large electrode bonding pads are farther to the two sides, separated by around 3 mm. To avoid possible inhomogeneities in composition and film degradation from

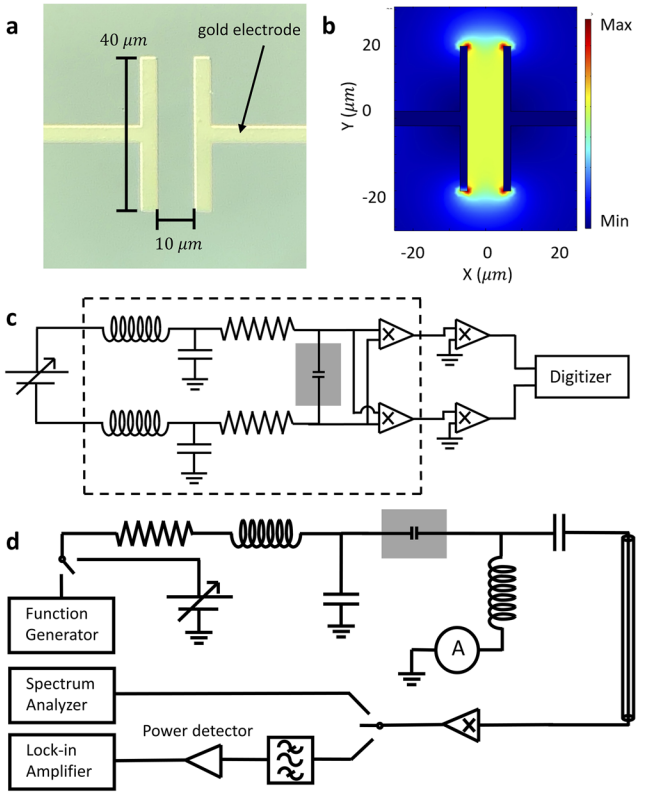

FIG. 1. (a) Optical microscope image of the 10 × 40 μm^2 device. The Au(70 nm)/V(7 nm) electrode are deposited on the surface of the V_2O_3 film, leaving a narrow gap with width height ratio equals 0.25. (b) The simulation from Comsol shows most of current (shown here in arbitrary units) is confined in the small region between the gap when the film resistivity is in the range explored in the present noise measurements. (c) Electrical circuit diagram of a low frequency noise measurement setup. The filtered constant current flows through the device, supplied by a programmable voltage source and current-limiting series resistors (1 MΩ each). Bias tees (C = 1 nF, L = 12 μH) prevent high frequency noise from the voltage source from reaching the sample. The voltage fluctuations across the sample (shaded rectangle) are amplified by two chains of preamplifiers in parallel; both amplifier chains are recorded by a high speed digitizer. The dashed line is the Faraday cage to shield the environmental noise. (d) Electrical circuit diagram of a high frequency noise measurement setup. Current bias is applied to the sample (shaded rectangle) using a voltage source, a function generator, and a current-limiting series resistor (20 kΩ). The high frequency signal and low frequency bias current are separated by bias tees (C = 1 nF, L = 12 μH). Function generator and lock-in amplifier combined to measure integral noise (225 MHz–580 MHz). High frequency spectra are recorded by a spectrum analyzer when applying constant current by a voltage source.

the etching process, the films were left intact, with electrode design and aspect ratio ensuring that the device conduction is limited by the interelectrode region [Figs. 1(a) and 1(b)]. Four device geometries ($10 \times 40\ \mu m^2$, $20 \times 80\ \mu m^2$, $40 \times 160\ \mu m^2$, and $80 \times 320\ \mu m^2$) were used such that two-terminal device resistances in the metallic state were nearly identical for all devices, but with varying current densities for the same applied bias. We note that the nearly identical resistances and noise magnitudes across the device geometries imply that the resistance and noise response are driven by the bulk of the film, rather than by contact effects.

B. Low-frequency noise measurement

Figure 1(c) shows the electrical circuit diagram of the low frequency experimental setup. A programmable voltage source (NI-DAQ6521) was followed by multiple LC filters to drive a clean dc current through two large current-limiting resistors (~1 MΩ each). The sample was mounted on a custom low frequency measurement probe and inserted into a cryostat (Quantum Design PPMS) with temperature stability better than 0.02% in the relevant temperature range. The measurement wirings are twisted pairs to reduce magnetic field induced noise. The sample, LC filters, transmission lines, and first pair of pre-amplifiers are shielded by a Faraday cage to reduce environmental noise. The voltage noise generated by the resistance fluctuations is collected by two separate amplifier chains, each consisting of two preamplifiers (NF LI-75 and Stanford Research SR-560). The two amplified signals are recorded by a high-speed data acquisition device (Picoscope 4262). Each time series containing 2 000 000 data points is taken with a sampling rate of 10 MHz. Cross correlation of the two time series data then reveals the voltage noise from the sample itself.[31] Unavoidable parallel parasitic capacitance comes from the sample mounting and cryostat wiring, leading to the capacitive suppression of measured voltage noise at high frequencies. This capacitive filtering can be calibrated and taken into account in analyzing the low frequency spectra. More details are provided in the supplementary material.

The thermal noise of different standard resistors was used to calibrate the setup. The voltage noise intensity found from the cross correlation can be expressed as $S_V = 4k_BTR \times A$, where the first factor is the Johnson–Nyquist voltage noise at the resistor R and A is the product containing the squared amplifier gain and a coefficient related to the cross-correlation parameters (the number of data points of each time series, the sampling frequency, and the windowing function used for the Fourier transform). The calibration procedure is discussed in greater detail in the supplementary material.

C. High-frequency noise measurement

We used two approaches to measure noise power at radio frequencies (RFs) [Fig. 1(d)], both requiring that the sample be mounted on a second custom probe with coaxial wiring and a RF-specialized sample carrier with integrated bias tee (1 nF capacitor and 12 μH inductor). The calibration of these approaches accounts for the RF response of the sample as terminating a transmission line/amplifier chain. In the first approach, we use high frequency amplification and a spectrum analyzer to record the frequency-dependent noise spectral density (10 MHz–1 GHz) directly. Effective bias tees allow the separation of current-biasing of the sample and measurements of the RF power. The voltage source (NI-DAQ6521) and current-limiting resistor provide a constant bias current through the sample, and the unfiltered signal is amplified by three RF power amplifiers (20 dB gain for each). The high frequency spectrum is recorded by a spectrum analyzer (E4402B), and each spectrum is averaged over 200 times. Greater details including the calibration procedure are provided in the supplementary material.

We also used a lock-in technique[32,33] to measure the integrated noise power from 225 MHz to 580 MHz. A square-wave bias (7.7 Hz) between 0 V and the desired bias voltage level is generated by a function generator (DS345) and applied to one side of the sample through a current-limiting resistor and LC circuit (to limit the current and suppress any extrinsic high frequency noise from the biasing setup, respectively). At the output port, the low frequency current flows through the inductor and is recorded by the combination of current amplifier (SR 570) and lock-in amplifier (SR 7265). The high frequency noise signal flows through the capacitor and is filtered by a low pass filter (<580 MHz) and a high pass filter (>225 MHz). The filtered signal is amplified by three RF power amplifiers (20 dB gain each) and detected by a power detector (Mini-Circuits zx47-60LN-S+ 10 MHz–8000 MHz). The integrated RF noise intensity is thus converted to a voltage signal and recorded by a lock-in amplifier (SR7270) synchronous with the square wave. Analogous to the low frequency approach, we used thermal noise of different value resistors to calibrate the high frequency setup. The calibration procedure details are in the supplementary material.

III. RESULTS

The DC conductivity of the V_2O_3 film devices was measured by recording the resistance during the cooling and warming cycles, using a source meter (Keithley 2400, 10 mV output). The temperature was held fixed for 5 min every 0.5 K through the transition to stabilize the device temperature. All devices responded similarly. Figure 2(a) shows the resistance changes with temperature in the cooling and warming cycles. In the cooling cycle, the antiferromagnetic insulating domains start to appear around 160 K and gradually replace the paramagnetic metallic domains. This transition happens rapidly with temperature between 150 K and 130 K, causing the resistance to increase by about four orders of magnitude. The resistance continues to increase to almost $10^7\times$ larger than that of the pure metallic phase when cooling down to 100 K. In the warming cycle, the transition from the antiferromagnetic insulating domains to the paramagnetic metallic domains is about 7 K higher than in the cooling cycle, showing thermal hysteresis. Beyond this thermal hysteresis that shifts R vs T, we found no apparent difference in conduction and noise measured at a given resistance upon warming and cooling. For consistency, the data presented below are all from cooling runs.

At each temperature for which we measured noise, the current–voltage (IV) characteristic is also recorded. At the low voltage bias range, as shown in Fig. 2(b), the IV curve is almost linear (see the inset for the log–log plot) and did not show any obvious hysteresis (either from possible current-induced changes in domain configuration or from heating coupled with thermal hysteresis), which ensures

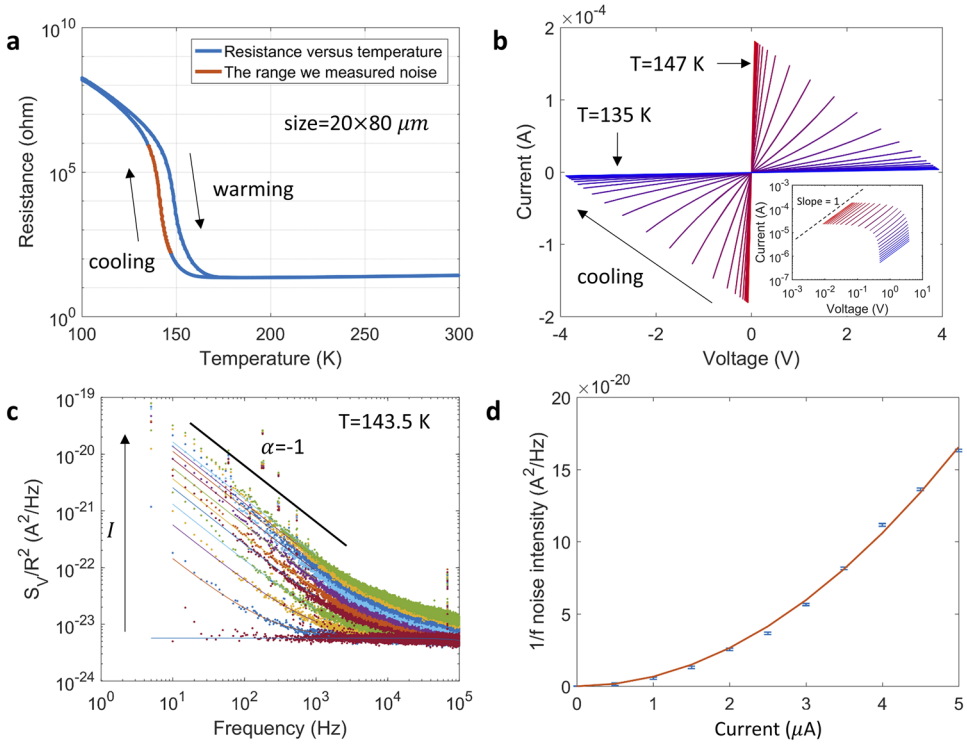

FIG. 2. (a) Resistance of a typical device vs temperature on cooling and warming cycles. (b) The *IV* curves in this small bias range at different temperatures are almost linear, as seen in the inset, which shows the same data in a log–log plot. (c) Typical spectra of low frequency noise at 143.5 K at successive equally spaced bias currents [indicated in (d)]. To distinguish spectra for different biases, each is plotted using different high contrast colors. The black line for comparison indicates a slope of −1. The bias range is from 0 μA to 5 μA. (d) Quadratic fitting of noise intensity at 1 Hz. The noise intensities and standard errors are from the 1/*f* noise fittings in (c). Each bias corresponds to one spectrum in (c). The dependence is of the form $y = ax^2$, where x is in μA and $a = 6.627 \pm 0.075 \times 10^{-21}$ $(A^2/Hz)/(\mu A^2)$.

noise spectra without complications due to bias-driven changes in thermal noise.

Figure 2(c) shows a T = 143.5 K typical low frequency noise spectrum at equally stepped bias currents, corrected for the capacitive roll-off and including the thermal noise background. The lowest (flat) spectrum corresponds to the zero bias thermal noise background. A slope of −1, corresponding to pure 1/*f* dependence, is indicated by the black line. Clearly, as bias is increased, a growing 1/*f*-like contribution to the total noise is apparent. [We note that while temperature fluctuations couple to the device resistance, variations in $T(t)$ cannot produce the observed spectra, neither the frequency dependence nor the current dependence. The thermal mass of the sample stage rules out temperature fluctuations on kHz and higher frequencies, and sample stage temperature control is independent of sample biasing conditions.]

For initial analysis, we assume a 1/*f* form for the low frequency noise to better highlight deviations from that form. The spectra are fitted with the following formula:

$$S_I(f) = \frac{S_V(f)}{R^2} = \frac{4k_BT/R + S_{1/f}/f}{1 + (2\pi fRC_P)^2}, \tag{1}$$

where $S_{1/f}$ is corresponding to the 1/*f* noise at frequency = 1 Hz at given current, R is the resistance of device, and $S_I(f) = \frac{S_V(f)}{R^2}$ is current noise. The term in the denominator accounts for parasitic capacitance C_P in the wiring, as discussed in the supplementary material. The contribution to the noise from a small resistance fluctuation $\delta R \ll R$ should have the form

$$I + \delta I = \frac{V}{(R + \delta R)} = \frac{V}{R} - \frac{V}{R} \times \frac{\delta R}{R},$$
$$(\delta I)^2 = \left(\frac{V}{R}\right)^2\left(\frac{\delta R}{R}\right)^2 = I^2\left(\frac{\delta R}{R}\right)^2. \tag{2}$$

This implies that the current noise from resistance fluctuations should be proportional to the square of the bias current, if the resistance fluctuations are independent of the magnitude of the bias current. The dependence of the inferred noise $S_{1/f}$ on bias is shown in Fig. 2(d). The quadratic relation between noise and current confirms that this low frequency noise contribution results from resistance fluctuations.

We now consider how those resistance fluctuations manifest at higher frequencies and at a different temperature, near the temperature for which the noise is maximized and Lorentzian deviations are seen from 1/*f* response. To compensate for different accessible bias current ranges in the low- and high-frequency measurement setups, we have used the observed quadratic dependence of noise on bias in both measurements. The low frequency spectra have had the zero bias thermal noise subtracted and are then scaled by a factor $\left(\frac{I_{max,high\ frequency}}{I_{max,low\ frequency}}\right)^2$ to permit comparison. Figure 3(a) shows the examples of the high frequency noise spectra (also with the zero-bias spectrum subtracted) at four equally stepped bias current values, on the same axes as normalized low frequency spectra.

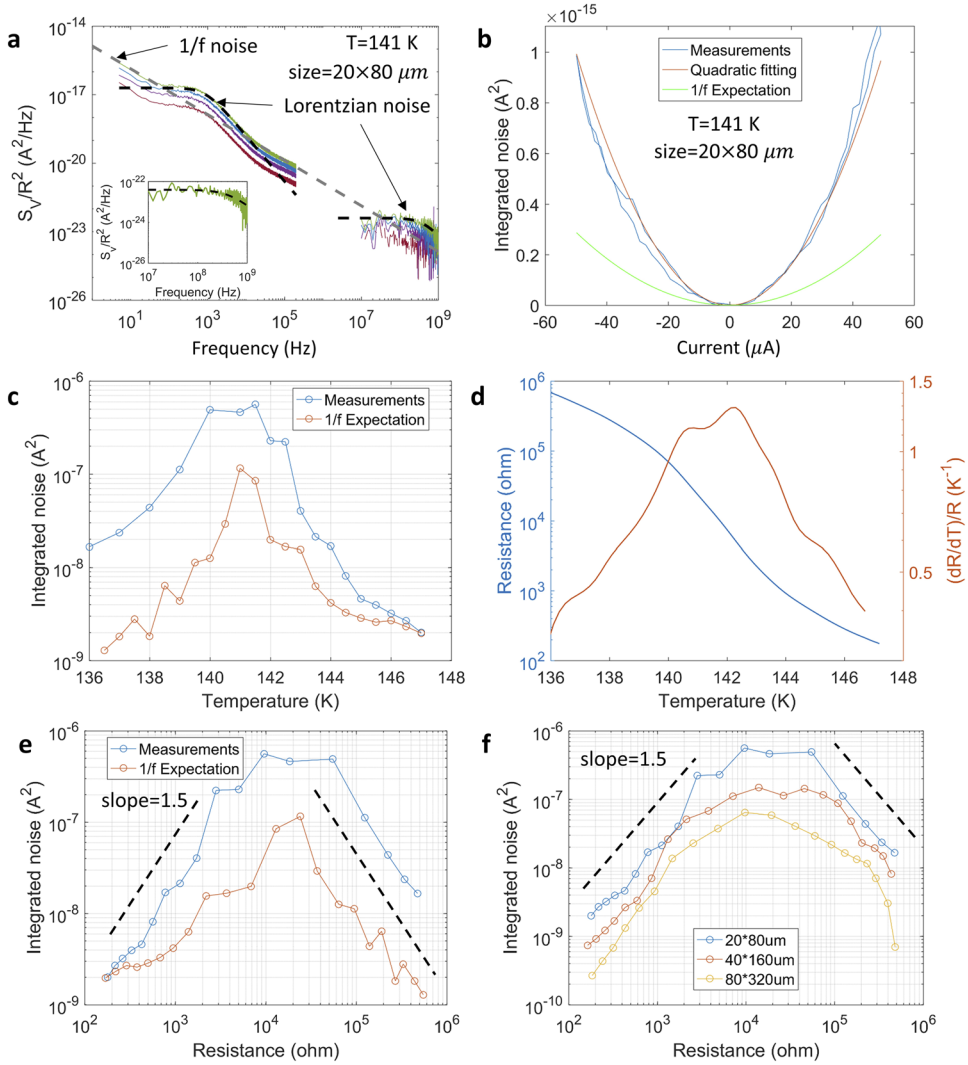

FIG. 3. (a) Normalized low frequency and high frequency spectra of the same device at 141 K (resistance ≈ 24 kΩ) at four different bias currents, near the temperature of maximum noise. The low frequency noise was acquired at a maximum current of 4.94 μA, and the high frequency noise was acquired at a maximum current of 105 μA. The normalized low frequency noise has had the thermal noise background subtracted and is multiplied by a factor of $(105/4.94)^2$ to scale for the quadratic current dependence of the noise and the current difference between the low and high frequency measurement setups. The three dashed lines show the 1/*f* low frequency noise and Lorentzian fits, one at low frequency and one at high frequency. The inset shows the highest bias spectrum of high frequency noise by itself for clarity. To distinguish spectra for different biases, the spectrum at each bias is plotted using different high contrast colors. (b) The integrated high frequency noise measured by a power detector (blue), a fit to a quadratic current dependence (red), and the expected integrated high frequency noise based on an extrapolation of the low frequency spectrum (green) at the same temperature assuming a 1/*f* frequency dependence. The dependence is of the form $y = ax^2$, where x is in μA and $a = 3.998 \pm 0.053 \times 10^{-19}$ $(A^2)/(\mu A^2)$. (c) For each temperature, the integrated noise measured by a RF power detector with a lock-in amplifier and the expected integrated noise over the same bandwidth based on an extrapolation of the low frequency noise assuming a 1/*f* frequency dependence. (d) For this same device, resistance R (decreasing blue curve, left axis) and normalized derivative $(dR/dT)/R$ (peaked red curve, right axis) as a function of temperature for a typical temperature cooldown. (e) The data of (c) plotted vs device resistance rather than temperature. The power laws shown by dashed lines are guides for comparison. (f) The integrated noise vs device resistance for different size devices, with power laws shown by dashed lines for comparison.

Two conclusions arise from these data. First, the high frequency noise is comparable to or larger than that expected from a simple 1/*f* extrapolation of the low frequency spectra. Second, from Fig. 3(a), Lorentzian noise (shoulder-shaped deviations from 1/*f* dependence) is observed in both the high frequency range and the low frequency range, implying that individual fluctuators are strongly affecting the total resistive fluctuations at this particular temperature where the noise is close to maximal. A typical Lorentzian noise has the form[34]

$$S_L(f) \propto \frac{\tau}{(2\pi f\tau)^2 + 1}, \tag{3}$$

where τ is the effective lifetime of the fluctuator. According to the fitting, the lifetime of the two dominant fluctuators shown in Fig. 3(a) are around 176 μs and 0.35 ns, with standard errors of fittings of low frequency and high frequency fluctuators 0.08 μs and 0.013 ns, respectively. More details about Lorentzian noise fitting and a discussion of the high frequency Lorentzian variability are provided in the supplementary material. Different heating and cooling cycles and different devices show different detailed fluctuator times. Tracing detailed temperature evolution of individual Lorentzian fluctuators is difficult, as these are most prevalent when the device resistance is changing most rapidly with temperature. Additional RF Lorentzian noise examples are shown in Fig. S7, and the inferred effective lifetimes range from 1 ns to 0.2 ns. As shown in Fig. S8, the Lorentzian deviations from $1/f$-like low frequency noise are most prevalent when the noise is near its maximum value; this is consistent with percolation expectations as described below.

We must check that the high frequency noise also results from resistance fluctuations. The RF lock-in detection method can increase the sensitivity at the cost of spectral information. Figure 3(b) shows the measurement of integrated noise measured at 141 K. The blue curve is measurement data, the red one is a quadratic fit, again showing consistency with the noise intensity in this frequency range being produced through resistive fluctuations. The green curve is a calculation based on fitting the low frequency noise to an expected $1/f$ dependence and extrapolating it to the RF bandwidth probed in the lock-in measurement. We routinely find that the measured RF signal is larger than the extrapolated expectation. This indicates the existence of more high frequency fluctuators than would be expected from either the usual $1/f$ noise or Lorentzian fluctuators at low frequencies.

Figure 3(c) shows the integrated noise and extrapolated low frequency $1/f$ noise expectation as a function of temperature. As shown in Fig. 3(d), the noise is maximized in the mixed phase regime approximately where the resistance is changing most rapidly with temperature, and much smaller (below our sensitivity to detect) in the fully metallic state. This is qualitatively typical of what has been seen in other mixed-phase metal–insulator transition systems.[20–22]

IV. DISCUSSION

Having clearly identified resistive noise at both low and high frequencies, it is worth comparing to the resistive noise seen in other material systems. The resistive noise, translated into voltage noise S_V via a bias current, is typically quantified by the Hooge relationship[28] $(S_V/(IR)^2)v_sf = \alpha/n$. For reference, the values of α/n found in disordered metals are 10^{-21} cm^3–10^{-23} cm^3 and 10^{-18} cm^3–10^{-21} cm^3 for semiconductors.[20,26] Surprisingly, in the mixed-phase regime of the $La_{5/8-x}Pr_xCa_{3/8}MnO_3$ MIT, α/n is as large as 10^{-10} cm^3–10^{-7} cm^3. In the VO_2 mixed phase regime,[22] in contrast, α/n is around 10^{-22} cm^3–10^{-24} cm^3, comparable to the disordered metal cases. Here, we find α/n is around 10^{-18} cm^3–10^{-20} cm^3, much larger than in VO_2, but comparable to observations in doped semiconductors. Further interpretation is challenging without additional assumptions of a microscopic model for the fluctuators, discussed below.

As mentioned, the metal–insulator transition mixed phase regime is often considered as a percolation problem, with the onset of metallicity corresponding to a percolating cluster of metallic domains.[20–23] Such clusters have been directly visualized in identically prepared V_2O_3 films using near field optical methods.[1] To compare with models of percolation, we examine the evolution of the noise intensity across the coexistence temperature regime. The maximum in noise occurring when the device resistance is most rapidly changing with temperature [Figs. 3(c) and 3(d)] is consistent with percolation. In scaling models of percolation,[11,14,20,26] there is a connection between percolation cluster size and resistive noise such that $S_V/(I)^2 \propto (p - p_c)^{-k}$, where p is the percolating phase fraction, p_c is the critical concentration, and k is a critical exponent. The peak in the noise intensity in Figs. 3(c) and 3(d) is consistent with this idea, since the total resistance is varying most rapidly when $p \sim p_c$.

To compare with different models of percolation, we can use the fact that in percolation, the resistance should also scale critically with p, with the resulting expectation that the normalized resistance noise $S_V/(IR)^2 \propto R^{-x}$, where x is another critical exponent. Figure 3(e) shows that x is close to 1.5 (the solid lines are not fits and are pure power laws for comparison only). In contrast, prior experiments studying VO_2 in the mixed phase regime showed x values of ~2.6 on both the insulating and metallic sides of the transition.[22] Differences in the resistive noise of the MIT between VO_2 and V_2O_3 are perhaps not surprising, given prior indications that the connections between structural and electronic transitions in the two oxides differ.[35,36]

A value of $x = 1.5$ on both sides of the mixed phase regime (metal-rich and insulator-rich) is quantitatively consistent with the predictions of a particular percolation model, the so-called "p-noise" in two dimensions.[16] In this approach, which is derived for a generic frequency dependence of the resistive noise $S_R(f)$, the material is modeled as a random network of resistors that have either a finite value (corresponding to a region of the metallic state) or an infinite resistance (corresponding to a region of the insulating state). For the system to qualify as two-dimensional, the characteristic lateral domain size should be comparable to or larger than the material thickness. In this model, the noise results from fluctuations that switch off or on connections between conducting regions (that is, fluctuations in the conducting fraction p) rather than changes in the resistance of the conducting regions themselves. An additional assumption is that the temperature dependence of the fluctuations in p is weak compared to the temperature dependence of the total resistance itself.

These V_2O_3 films are good candidates for observing p-noise. There is a four orders of magnitude or more contrast in the resistivity between the metallic and insulating domains. Nanoscale infra-red near-field experiments[1] in such films in the mixed phase regime near the percolation threshold have shown lateral domain sizes on the order of hundreds of nanometers, implying that the present films comply with the model's definition of 2D. The observation of Lorentzian noise near the percolation threshold [Fig. 3(a) and Fig. S8] is also consistent; p fluctuating between two values with the system near the percolation threshold (e.g., an individual fluctuating region located at a key juncture in the percolating cluster) would be expected to generate Lorentzian noise. The broadband measurements that produced the data in Figs. 3(e) and 3(f) are essentially averaging the frequency-dependent resistive noise over the high frequency bandwidth. Since p-noise is derived for a generic frequency

dependence, the power law relationship x would be expected to hold for such an average.

In light of this experimental consistency with p-noise model expectations, it is worth considering how the physics of the MIT constrains possible fluctuation mechanisms. That is, what is actually fluctuating to give changes in p? In thermal equilibrium at temperature T, statistical mechanics in the canonical ensemble shows that the mean square energy content fluctuations of a volume v are given by $(\delta E)^2 = (C_v v)k_B T^2$, where C_v is the specific heat per unit volume. If the resistance fluctuations result from some thermally fluctuating volume v being fully converted between metallic and insulating structural phases that would require $\delta E \sim Lv$, where L is the latent heat per unit volume, 65 J/cm^3.[37] Rearranging, $v \sim (C_v/L^2)k_B T^2$. Assuming that the lattice specific heat dominates (~3.2 J/K cm^3 [38]) and T = 150 K gives a typical volume scale of 240 Å^3, comparable in volume to a single unit cell. This and the hysteretic nature of first-order transitions imply that it is unlikely that the resistance fluctuations involve complete switching of metallic or insulating domains. The thermal energy available in a typical fluctuation should only be sufficient to shift phase boundaries by a couple of lattice spacings. From nanooptical characterization of percolation in this system,[1] with comparatively large (hundreds of nm in lateral extent) domains, it is unclear whether such small characteristic distances would be able to alter the connectivity of the conducting network sufficiently to explain the relevance of the p-noise model and the measured noise intensity. The relevant fluctuations would have to be at domain boundaries, altering the connectivity of the metallic domain network. As noted above, the appearance of Lorentzian noise in the measurements, particularly near the maximum in noise amplitude at the percolation threshold [Fig. 3(a) and Fig. S8], does suggest that small numbers of fluctuators can have a strong influence on the connectivity of the network as a whole.

More speculatively, rather than complete structural transitions of volumes between the metallic and insulating phases, an alternative possible source of resistive fluctuations and changes in the connectivity of conducting regions could be scattering of carriers by fluctuating antiferromagnetism, as the system sits at the boundary between the paramagnetic metal and the AFM insulator. AFM fluctuations have been observed in the metallic state of V_2O_3,[39] and recently signatures of such fluctuations were also observed in the insulating state[40] and have also been linked to transport properties through magnetoresistance measurements.[41] Slow fluctuations of AFM domains[42] lead to $1/f$ noise in metallic Cr around and below the bulk Neel temperature.[43] The detection of resistive fluctuations up to the short timescales accessed in the present experiments further constrain possible fluctuation mechanisms to those compatible with such rapid dynamics.

We also compare the noise intensity for different size devices; the results are shown in Fig. 3(f). For larger devices, the noise due to resistive fluctuations is smaller, presumably due to ensemble averaging over the larger device area. In the smallest devices in which the current densities and electric fields are largest, the lock-in measurement of integrated high frequency noise shows pronounced deviations from a quadratic dependence of the noise intensity with bias current [Figs. S4(a) and S4(b)]. The measured noise shows instabilities at high biases (not readily apparent in the current–voltage characteristic itself) and tends toward a superquadratic dependence on current. These traits indicate that at the high current/field limit, the current itself is no longer serving as a nonperturbative probe of resistance fluctuations but instead is driving domain dynamics, including those at hundreds of MHz.

V. SUMMARY

We measured resistance noise in V_2O_3 films at both low frequency and radio frequency ranges across the mixed-phase range of the metal–insulator transition. The variation of the noise with the total resistance across the transition is quantitatively consistent with a p-noise model of 2D percolation in which the noise arises from temporal fluctuations in the percolating fraction of the conducting medium. Lorentzian noise was observed, particularly near the temperature when noise was maximized, in both low frequency and radio frequency ranges. This Lorentzian noise shows the importance of individual fluctuators when the metallic domains are near the percolation threshold. The inferred lifetime of fast fluctuators varies from 1 ns to 0.2 ns, approaching the timescale associated with the photo-induced insulator-to-metal transition.[9] The thermodynamics of the MIT suggests that fluctuations of entire domains between the equilibrium metallic and insulating structural phases are unlikely to be the source of the resistive noise; rather, fluctuations of volumes that alter connectivity at domain boundaries operate. These noise results call for further examination of the electronic and magnetic dynamics in the mixed phase regime at the nanoscale and high frequency scales. Noise of the kind presented here may serve as a sensitive and nonperturbative probe for the dynamics of switching phenomena in this system, providing complimentary information, which cannot be obtained by perturbative pump–probe experiments. Understanding these intrinsic fluctuation dynamics in this and related systems is of fundamental interest and necessary for neuromorphic applications of metal–insulator transitions.[7,44]

SUPPLEMENTARY MATERIAL

See the supplementary material for calibration procedures of both low and high frequency measurements, comparison with data from other device sizes, and further discussion of the Lorentzian features.

ACKNOWLEDGMENTS

The authors acknowledge M. J. Rozenberg for helpful conversations. D.N., L.C., and P.Z. acknowledge support from DOE BES (Award No. DE-FG02-06ER46337). Some of the noise measurement hardware was acquired through the NSF (Grant No. DMR-1704264). Y.K. and I.K.S. acknowledge support from the Vannevar Bush Faculty Fellowship program sponsored by the Basic Research Office of the Assistant Secretary of Defense for Research and Engineering and funded by the Office of Naval Research (Grant No. N00014-15-1-2848).

DATA AVAILABILITY

The data that support the findings of this study are available from the corresponding author upon reasonable request.

REFERENCES

[1] A. S. McLeod, E. van Heumen, J. G. Ramirez, S. Wang, T. Saerbeck, S. Guenon, M. Goldflam, L. Anderegg, P. Kelly, A. Mueller, M. K. Liu, I. K. Schuller, and D. N. Basov, Nat. Phys. **13**, 80 (2016).

[2] D. B. McWhan and J. P. Remeika, Phys. Rev. B **2**, 3734 (1970).

[3] E. Abreu, S. Wang, J. G. Ramírez, M. Liu, J. Zhang, K. Geng, I. K. Schuller, and R. D. Averitt, Phys. Rev. B **92**, 085130 (2015).

[4] G. Lantz, B. Mansart, D. Grieger, D. Boschetto, N. Nilforoushan, E. Papalazarou, N. Moisan, L. Perfetti, V. L. R. Jacques, D. Le Bolloc'h, C. Laulhé, S. Ravy, J.-P. Rueff, T. E. Glover, M. P. Hertlein, Z. Hussain, S. Song, M. Chollet, M. Fabrizio, and M. Marsi, Nat. Commun. **8**, 13917 (2017).

[5] N. Alyabyeva, J. Sakai, M. Bavencoffe, J. Wolfman, P. Limelette, H. Funakubo, and A. Ruyter, Appl. Phys. Lett. **113**, 241603 (2018).

[6] P. Limelette, A. Georges, D. Jérome, P. Wzietek, P. Metcalf, and J. M. Honig, Science **302**, 89 (2003).

[7] J. del Valle, P. Salev, F. Tesler, N. M. Vargas, Y. Kalcheim, P. Wang, J. Trastoy, M.-H. Lee, G. Kassabian, J. G. Ramírez, M. J. Rozenberg, and I. K. Schuller, Nature **569**, 388 (2019).

[8] M. K. Liu *et al.*, Phys. Rev. Lett. **107**, 066403 (2011).

[9] A. Singer, J. G. Ramirez, I. Valmianski, D. Cela, N. Hua, R. Kukreja, J. Wingert, O. Kovalchuk, J. M. Glownia, M. Sikorski, M. Chollet, M. Holt, I. K. Schuller, and O. G. Shpyrko, Phys. Rev. Lett. **120**, 207601 (2018).

[10] J. del Valle, J. G. Ramírez, M. J. Rozenberg, and I. K. Schuller, J. Appl. Phys. **124**, 211101 (2018).

[11] R. Rammal, C. Tannous, P. Breton, and A.-M. S. Tremblay, Phys. Rev. Lett. **54**, 1718–1721 (1985).

[12] R. H. Koch, R. B. Laibowitz, E. I. Alessandrini, and J. M. Viggiano, Phys. Rev. B **32**, 6932 (1985).

[13] J. V. Mantese and W. W. Webb, Phys. Rev. Lett. **55**, 2212 (1985).

[14] A.-M. S. Tremblay, S. Feng, and P. Breton, Phys. Rev. B **33**, 2077 (1986).

[15] M. Octavio, G. Gutierrez, and J. Aponte, Phys. Rev. B **36**, 2461 (1987).

[16] L. B. Kiss and P. Svedlindh, Phys. Rev. Lett. **71**, 2817 (1993).

[17] C. Pennetta, G. Trefán, and L. Reggiani, Phys. Rev. Lett. **85**, 5238 (2000).

[18] O. Cohen, Z. Ovadyahu, and M. Rokni, Phys. Rev. Lett. **69**, 3555 (1992).

[19] J. Jaroszyński, D. Popović, and T. M. Klapwijk, Phys. Rev. Lett. **89**, 276401 (2002).

[20] V. Podzorov, M. Uehara, M. E. Gershenson, T. Y. Koo, and S.-W. Cheong, Phys. Rev. B **61**, R3784 (2000).

[21] B. Raquet, A. Anane, S. Wirth, P. Xiong, and S. von Molnár, Phys. Rev. Lett. **84**, 4485 (2000).

[22] Z. Topalian, S.-Y. Li, G. A. Niklasson, C. G. Granqvist, and L. B. Kish, J. Appl. Phys. **117**, 025303 (2015).

[23] A. L. Rakhmanov, K. I. Kugel, Ya. M. Blanter, and M. Yu. Kagan, Phys. Rev. B **63**, 174424 (2001).

[24] F. N. Hooge, T. G. M. Kleinpenning, and L. K. J. Vandamme, Rep. Prog. Phys. **44**, 479 (1981).

[25] M. B. Weissman, Rev. Mod. Phys. **60**, 537 (1988).

[26] S. Kogan, *Electronic Noise and Fluctuations in Solids* (Cambridge University Press, Cambridge, England, 1996).

[27] C. T. Rogers and R. A. Buhrman, Phys. Rev. Lett. **53**, 1272 (1984).

[28] F. N. Hooge and L. K. J. Vandamme, Phys. Lett. A **66**, 315 (1978).

[29] J. Trastoy, Y. Kalcheim, J. del Valle, I. Valmianski, and I. K. Schuller, J. Mater. Sci. **53**, 9131 (2018).

[30] Y. Kalcheim, N. Butakov, N. M. Vargas, M.-H. Lee, J. del Valle, J. Trastoy, P. Salev, J. Schuller, and I. K. Schuller, Phys. Rev. Lett. **122**, 057601 (2019).

[31] A. Kumar, L. Saminadayar, D. C. Glattli, Y. Jin, and B. Etienne, Phys. Rev. Lett. **76**, 2778 (1996).

[32] F. Wu, L. Roschier, T. Tsuneta, M. Paalanen, T. Wang, and P. Hakonen, AIP Conf. Proc. **850**, 1482 (2006).

[33] M. Reznikov, M. Heiblum, H. Shtrikman, and D. Mahalu, Phys. Rev. Lett. **75**, 3340 (1995).

[34] A. V. Kuhlmann, J. Houel, A. Ludwig, L. Greuter, D. Reuter, A. D. Wieck, M. Poggio, and R. J. Warburton, Nat. Phys. **9**, 570 (2013).

[35] J. G. Ramirez, T. Saerbeck, S. Wang, J. Trastoy, M. Malnou, J. Lesueur, J.-P. Crocombette, J. E. Villegas, and I. K. Schuller, Phys. Rev. B **91**, 205123 (2015).

[36] S. Wang, J. G. Ramírez, and I. K. Schuller, Phys. Rev. B **92**, 085150 (2015).

[37] H. V. Keer, D. L. Dickerson, H. Kuwamoto, H. L. C. Barros, and J. M. Honig, J. Solid State Chem. **19**, 95 (1976).

[38] E. Abreu, S. N. Gilbert Corder, S. J. Yun, S. Wang, J. G. Ramírez, K. West, J. Zhang, S. Kittiwatanakul, I. K. Schuller, J. Lu, S. A. Wolf, H.-T. Kim, M. Liu, and R. D. Averitt, Phys. Rev. B **96**, 094309 (2017).

[39] W. Bao, C. Broholm, G. Aeppli, P. Dai, J. M. Honig, and P. Metcalf, Phys. Rev. Lett. **78**, 507 (1997).

[40] B. A. Frandsen, Y. Kalcheim, I. Valmianski, A. S. McLeod, Z. Guguchia, S. C. Cheung, A. M. Hallas, M. N. Wilson, Y. Cai, G. M. Luke, Z. Salman, A. Suter, T. Prokscha, T. Murakami, H. Kageyama, D. N. Basov, I. K. Schuller, and Y. J. Uemura, Phys. Rev. B **100**, 235136 (2019).

[41] J. Trastoy, A. Camjayi, J. del Valle, Y. Kalcheim, J.-P. Crocombette, J. E. Villegas, M. Rozenberg, D. Ravelosona, and I. K. Schuller, Phys. Rev. B **101**, 245109 (2020).

[42] O. G. Shpyrko, E. D. Isaacs, J. M. Logan, Y. Feng, G. Aeppli, R. Jaramillo, H. C. Kim, T. F. Rosenbaum, P. Zschack, M. Sprung, S. Narayanan, and A. R. Sandy, Nature **447**, 68 (2007).

[43] R. P. Michel, N. E. Israeloff, M. B. Weissman, J. A. Dura, and C. P. Flynn, Phys. Rev. B **44**, 7413 (1991).

[44] Y. Kalcheim, A. Camjayi, J. del Valle, P. Salev, M. Rozenberg, and I. K. Schuller, Nat. Commun. **11**, 2985 (2020).